Developing a collaborative control strategy of a combined radiant floor cooling and ventilation system: A PMV-based model

Jing Ren[1], Jiying Liu[1,2,*], Shiyu Zhou[1], Moon Keun Kim[3], Jikui Miao[4]

[1]School of Thermal Engineering, Shandong Jianzhu University, Jinan 250101, China

[2]Built Environment Design and Research Institute, Shandong GRAD Group, Dezhou 253000, China

[3]Department of Civil Engineering and Energy Technology, Oslo Metropolitan University, Oslo N-0130, Norway

[4]School of Architecture and Urban Planning, Shandong Jianzhu University, Jinan 250101, China

*Corresponding author email: jxl83@sdjzu.edu.cn

Abstract

The development of collaborative control strategies for radiant cooling and ventilation systems improves thermal comfort and energy efficiency. This study used the Transient System Simulation (TRNSYS) tool integrated with the parametric simulation manager jEPlus to determine the optimal starting and operation mode of a combined radiant floor cooling (RFC) and ventilation system. The results were validated by an experiment. The optimization process was constrained by the thermal comfort defined by the predicted mean vote (PMV) with the objective of minimizing energy consumption. The results showed that the ventilation system was started one hour earlier than the RFC system at an initial indoor humidity of 85% to prevent condensation, whereas both systems were started at the same time at 75% in the starting stage. In the operation stage, the self-regulation potential of the RFC system and the adjustment of the cooling capacity of the ventilation system were coordinated to counter dynamic internal heat gains. Moreover, the proportion of the total sensible heat removed by the RFC system to the total sensible heat removed by the ventilation system (S_v/S_R) was positively correlated with the total energy consumption. The S_v/S_R must be sufficiently high to prevent a large PMV deviation from the comfort zone of -0.5 to 0.5. A collaborative control strategy using the PMV-based model was proposed to adjust the S_v/S_R according to the PMV range, resulting in a highly efficient operation and maximum energy savings of 26.2%.

Keywords: radiant floor cooling, ventilation system, collaborative control strategy, PMV-based model

Highlights

- The starting and operation modes of a combined radiant cooling and ventilation system were studied.
- The correlation between PMV, S_v/S_R, and energy consumption was investigated.
- A collaborative control strategy was proposed to enhance the coordination of both systems.
- Adjusting S_v/S_R based on a PMV-based model improved energy efficiency and control accuracy.

1 Introduction

Radiant cooling has undergone extensive technological advancements in recent years and represents a novel cooling approach. It has attracted increasing attention because it provides high indoor comfort and low energy consumption [1,2]. In addition, the use of radiant cooling has increased with the development of high-temperature cooling [3,4]. However, since the radiant terminal can only provide indoor temperature regulation, it is necessary to install a ventilation system to supply fresh air and dehumidify the air. Thus, a cooling terminal is typically used to control the indoor thermal environment [5-7].

As an effective method of indoor temperature regulation, radiant cooling is achieved by convective and radiative heat transfer between a radiant surface and the indoor surface, occupants, equipment, and lights [8,9]. A radiant cooling system can maintain a stable indoor environment, is energy efficient, and provides a high-temperature cooling mode [10,11]. In addition, the radiative heat transfer between the human body and radiant surfaces ensures sufficient thermal comfort at higher indoor air temperatures [12]. Radiant systems with large surface areas and small temperature differences between surfaces and the indoor air temperature have a significant level of self-regulation [13]. A slight change in room temperature results in a significant difference in the heat

DOI: https://doi.org/10.1016/j.jobe.2022.104648

exchange amount. However, the self-regulation of the radiant cooling system cannot compensate for large thermal variation [14]. Besides, it is infeasible to implement conventional control strategies to deal with changes in the room temperature due to the high thermal inertia of the radiant cooling system [15]. Therefore, the dynamic thermal characteristics of a radiant structure must be analyzed to achieve accurate and efficient control of radiant cooling systems.

Several measures can be used to take advantage of the thermal inertia of the radiant terminal and overcome its negative effect. A radiant cooling/heating system has the potential to shift building load for energy conservation due to the large thermal inertia [16]. It is often operated asynchronously with the cooling loads of the building [17,18]. When the radiant cooling system is shut down, heat is accumulated in the radiant structure. Pre-cooling is required to reduce the indoor residual heat load and remove accumulated heat from the radiant structure. due to radiant system with large thermal mass [6]. A sufficient precooling time of the radiant terminal is required to ensure acceptable thermal comfort at the beginning of the occupancy period. Due to the thermal mass of the radiant structure, the continuous operation with a very low or very high supply water temperature results in undercooling or overheating problems. These problems can be solved by limiting the operation time or operating the circulation pump intermittently [19]. It has also been suggested to apply a variable temperature control method that provides high control precision for a wide range of partial loads and a relatively uniform surface temperature distribution across the radiant panel [20]. Inspired by the feasibility of using high thermal inertia of the radiant panel to mitigate the effect of frequent fluctuations in water temperature, Tang et al. [21] proposed a novel pulsed flow control method based on intermittent control with a fixed and short on-time duration to control the indoor temperature by determining the on-off ratio of the valve in a fixed short control cycle. However, the high thermal inertia of the radiant structure causes a limited response rate and a delayed response to the sudden increase in indoor heat gain [13]. Using radiant cooling alone to maintain air set-point temperature possibly often caused the condensation problem [22].

Radiant cooling systems should be combined with a ventilation system to control the indoor thermal environment and meet the cooling requirement of air-conditioned rooms [23]. The ventilation system provides dehumidification to maintain an appropriate indoor humidity level and improves the cooling capacity of the composite cooling system [24,25]. Since condensation often occurs during the start-up period of the radiant cooling system, it has been recommended to start the ventilation system first and the radiant cooling system second. It has also been reported that the ventilation system should be started at least one hour earlier than the radiant cooling system to prevent condensation [26]. In addition, the proportion of heat load removed by the ventilation system to the total heat load is a critical control parameter. A low heat load removed by a displacement ventilation (DV) system creates low thermal stratification, improving indoor thermal comfort [27]. It was observed that the radiant cooling system removed the major portion of the sensible load, providing satisfying indoor thermal comfort. No drafts occurred during the system's operation if the heat removal by the chilled ceiling system was less than 100 W/m^2 [28]. Outdoor air ventilation can also be used to ensure indoor thermal comfort [29]; the load handling tasks should be determined by the relationship between the outdoor and indoor temperature and humidity. A composite cooling system can achieve high cooling performance due to the positive influence of supplementary cooling by the ventilation system [30].

Most existing studies have focused on the operational control of the hydronic sides of radiant cooling systems, but there is a lack of discussion on collaborative control strategies for radiant cooling and ventilation systems. In some cases, the cooling capacity of radiant systems was impaired due to the simple control of the radiant surface temperature to prevent condensation without coordinating the ventilation system. Meanwhile, only regulating the chilled water parameters of the radiant systems cannot prevent highly dynamic internal heat gains. This approach can cause undercooling or overheating of a room and low energy efficiency. Moreover, advanced

controls such as PMV-based controls have been increasingly used for radiant cooling systems but require improvements in accuracy and efficiency.

The studies on collaborative control strategies and PMV-based control are summarized in Table 1. These studies commonly used PMV index to evaluate thermal comfort for radiant cooling systems. The relationship between the thermal comfort characteristics and other parameters related to the indoor environment and system operation was investigated to provide references for system design. The application of PMV was only limited to evaluate the thermal comfort conditions provided by radiant cooling systems. Therefore, it is necessary to improve the use of PMV by integrating it into control mechanism for the radiant cooling system. The system control required considering thermal comfort to represent direct physical and psychological occupant response to indoor environmental conditions.

Moreover, traditional air temperature-based control methods cannot precisely provide occupant thermal sensation and other indoor parameters [31]. Monitoring temperature alone is unable to reveal acceptable temperatures caused by adaptation to high humidity [32]. Since unique heat transfer mode of radiant cooling led to different indoor thermal environment, the commonly used indoor temperature setpoint was inapplicable to fulfill comfort requirement. Consequently, the PMV-based control model considering indoor air temperature, air humidity, air velocity, mean radiant temperature, clothing insulation level, and human activity can be an effective way to improve the thermal comfort, as well as reducing the energy and cost for buildings [33].

Table 1

A summary of PMV-based control for combined radiant cooling and ventilation systems.

Reference	System type	Method	Indices	Key findings
Saber et al. 2014 [34]	Radiant ceiling panel and decentralized dedicated outdoor air system	Experiment	PMV, PPD	The sensible cooling load of the space has a stronger impact than the supply water temperature on the cooling capacity of radiant ceiling panels.
Zarrella et al. 2014 [35]	Radiant floor cooling and dehumidification systems	Computer simulation	PMV	The water temperature control, based on the dew point of room air, and the interaction between radiant cooling power and supply air cooling conditions, require a specific overall analysis, when radiant floor cooling was coupled with dehumidification.
Bayoumi et al. 2018 [5]	Radiant cooling panel on the sidewall and mechanical ventilation air	IDA-ICE, numerical simulation	PMV	Integrating passive and active cooling and ventilation solutions helps maintaining the dewpoint temperature within desired limits over the radiant surface temperature, and results in healthier and more comfortable spaces.
Qin et al. 2020 [36]	Radiant cooling panel on ceiling and walls and dedicated fresh-air system	Numerical simulation	PMV, PPD	The optimum radiant surface temperature is 19 °C to 23 °C when fresh-air supply temperature is 26 °C. The relative humidity should be maintained at 50% to 70%, and the area ratio of radiant panels to total surfaces should be kept within 0.15 to 0.38 when the radiant surface temperature is 20 °C and the fresh-air supply temperature is 26 °C.
Gu et al. 2021 [37]	Radiant floor cooling and fan coil	Experiment	PMV, PPD	The novel radiant air conditioning system can handle transient heat and humidity load changes, improve the response speed of the radiant system, and meet the needs of intermittent use.
Hu et al. 2022 [38]	Capillary radiant cooling system with	TRNSYS simulation	PMV	When the radiant cooling system is operating intermittently, it is necessary to

fresh air supply	tool	control the dry-bulb temperature and dew-point temperature simultaneously in the unoccupied period to ensure indoor comfort and the smooth operation of radiant systems.

The exiting control for a composite system commonly used the regulation of supply water temperature and flow rate coupled with supply air temperature and flow rate. The independent cooling load handling method of a radiant cooling system and a ventilation ignored the relation between radiative and convective heat transfer, negatively affecting system efficiency and performance. It was found that the cooling load sharing rate represents the proportion of cooling load removed by a radiant cooling system to that removed by a ventilation system [1], therefore, adjusting cooling load sharing rate can enhance coordination of both systems to effectively deal with variable indoor heat gains so as to achieve energy saving potential and highly efficient operation. Moreover, an in-depth analysis of the collaborative operation of the combined RFC system and ventilation system is required. The novelty of this study is using PMV-based model instead of traditional air temperature-based mode in the control process of the radiant cooling system combined with ventilation system to determine suitable cooling load sharing rate to exploit the interaction of the convective and radiative heat transfer for cooling. In the end, a collaborative control strategy is established to improve control accuracy and prevent energy waste.

In this study, the Transient System Simulation (TRNSYS) tool and the parametric simulation manager jEPlus were used to simulate the starting stage and operation stage of a combined RFC and ventilation system. The aim is to combine dynamic and static control by coordinating the tasks of the RFC system and ventilation system to exploit the advantages of each system. The optimal control of the system prevents thermal discomfort and unnecessary energy consumption caused by a delay and a mismatch between the cooling energy supply and the load demand. The simulation results, including the indoor environmental parameters, predicted mean vote (PMV), and energy consumption, were analyzed to evaluate the effects of various indoor and outdoor parameters to make suitable adjustments to the cooling energy supply. The correlation between the PMV, the proportion of the sensible heat load removed by the RFC system to the sensible heat load removed by the ventilation system (S_v/S_R), and energy consumption was analyzed to derive the S_v/S_R adjustment strategy. The influences of different operational parameters on the PMV and energy consumption were obtained to make reasonable adjustments to the operational parameters based on the variable total cooling energy demand. Furthermore, a PMV-based model was created with indoor thermal comfort constraints to minimize energy consumption and used to develop a S_v/S_R adjustment strategy to achieve the collaborative control of the combined RFC and ventilation system.

2 Methodology

2.1 Research framework

The flowchart of this research is illustrated in Fig. 1. The TRNSYS integrated with jEPlus were used to optimize the control strategy of a combined RFC and ventilation system with different operational parameters in the starting stage and operation stage. A building model equipped with the composite cooling system was established in TRNSYS as the basic simulation model. Based on the building load characteristic and system performance, values for the selected parameters were defined in jEPlus to create different simulation cases. These cases were used as input into the TRNSYS for calculation, and the simulation results were obtained by jEPlus. The effects of the different operational parameters were determined, and the correlation between S_v/S_R, PMV, and energy consumption was obtained. A PMV-based model was established to implement the optimized control strategy of the composite system.

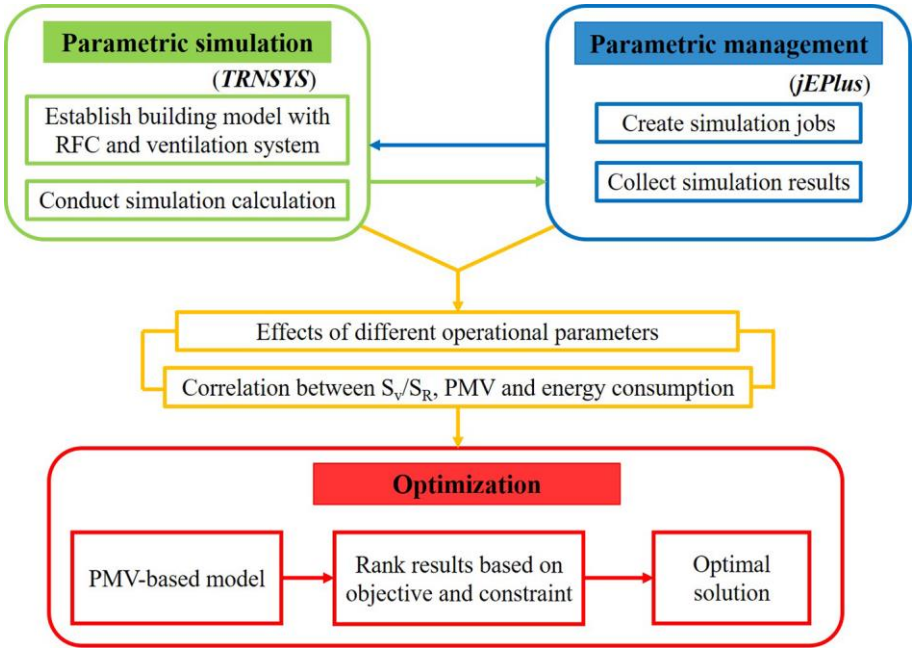

Fig. 1. Flow chart of the research.

2.2 Simulation tool

TRNSYS have been widely used to analyze energy consumption and determine building control and operation schemes [39]. A simplified model of the air conditioning system was implemented using the multizone building module Type 56 to carry out the dynamic simulation of the designed cases. The Type 56 energy balance model is described as shown in Fig. 2 [40]. The heat balance is defined as the correlation between the change rate of the internal thermal energy of the air node, the net heat gain caused by different heat transfer rates, and the power output of the air node as shown in Eq. (1) [40].

$$\frac{C_i}{\Delta t}\left(T_{set,i} - T_{\tau-\Delta t}\right) = Q_{surf,i} + Q_{env,i} + Q_{inf,i} + Q_{int,i} + Q_{solar,i} - P_i \quad (1)$$

where C_i is the thermal capacitance of air node i; $T_{set,i}$ denotes the set temperatures for heating or cooling in air node i; $Q_{surf,i}$ is the radiative and convective gain from the surfaces; $Q_{env,i}$ is the gain due to air entering air node i across walls; $Q_{inf,i}$ is the infiltration gain; $Q_{int,i}$ are the radiative and internal convective gains (by people, equipment, lighting radiators, etc.); $Q_{solar,i}$ is the solar radiation gain through the windows; P_i is the power output for heating or cooling.

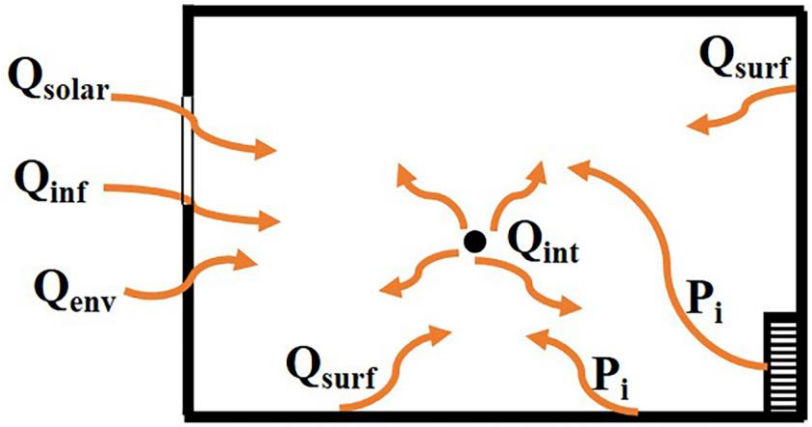

Fig. 2. Schematic diagram of the Type 56 energy balance model [40].

The moisture balance is calculated by considering the humidity ratios with or without

humidification/dehumidification for a certain set-point. The buffer effect is considered by using the effective moisture capacitance. The moisture balance of an air node is described by Eq. (2) [40].

$$M_{eff,i}\frac{d\omega_i}{dt} = m_{inf,i}(\omega_a - \omega_i) + \sum_k^{nvent} m_{v,k,i}(\omega_{v,k,i} - \omega_i) + W_{int,i} + \sum_{i-j} m_{env}(\omega_j - \omega_i) \quad (2)$$

where $M_{eff,i}$ is the effective moisture capacitance of the air node i; ω_i is the humidity ratio of the air node i; m_{inf} is the mass flow rate of infiltration air; ω_a is the ambient humidity ratio; $m_{v,k,i}$ is the mass flow rate of ventilation air; $\omega_{v,k,i}$ is the humidity ratio of the ventilation air; $W_{int,i}$ is the internal moisture gain; m_{env} is the mass flow rate of air entering air node i across walls; ω_j is the humidity ratio of air entering air node i across walls.

An active layer was used to model the radiant floor. This layer type contained fluid-filled pipes transferring heat from the radiant surface. The heat transfer between the radiant surface and indoor air depended on the active layer temperature. Moreover, Type 56 provided the ventilation type to specify the supply airflow for cooling. A simple model was established to replace the air handling unit to handle the supply airflow to the required inlet conditions. It should be noted that both the active layer and the ventilation type used internal calculations of Type 56 to obtain the energy demand.

jEPlus is a parametric tool to connect with TRNSYS using the DCK file [41]. The parameter values were defined in jEPlus to create simulation jobs. This was implemented in a recursive manner through the tree-like structure to list all possible paths from the root to the leaves. Each job contained a unique set of parameter values that were saved in the DCK file. The job list was sent to TRNSYS for the calculation of different simulation jobs with different design parameters values. All simulation results were transferred back to jEPlus to enable complex parametric analyses as shown in Fig. 3.

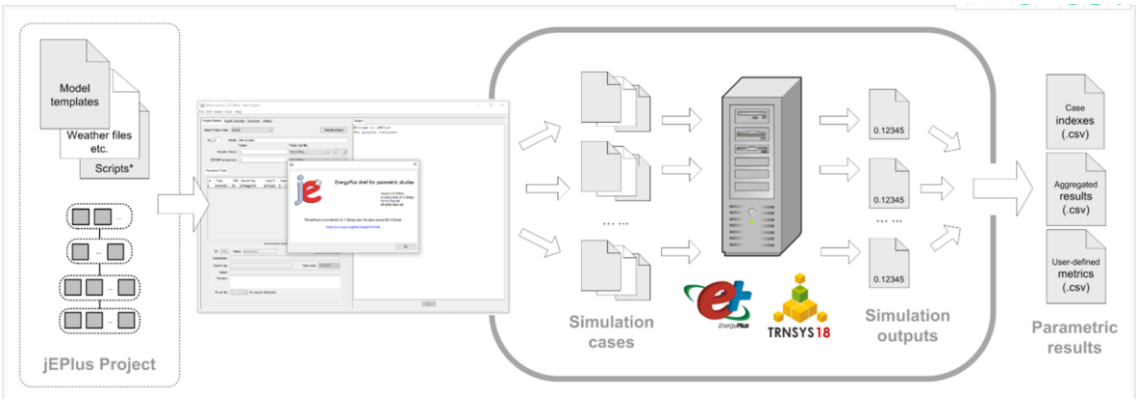

Fig. 3. Schematic diagram of the jEPlus simulation [41].

2.3 Simulation model

The building model was established according to an office building in Jinan [18]. The location and side view of the office building are depicted in Fig. 4. The physical and geometric parameters of the building were taken from the information of the actual office building [42]. The U-values for the exterior wall, the roof, and the exterior windows were 0.6 W/(m^2·K), 0.55 W/(m^2·K), and 2.4 W/(m^2·K), respectively. A south-facing room on the fifth (top) floor of the office building was selected to study the operational control of the RFC and ventilation system. The room had an air conditioning area of 50 m^2, two exterior windows, and one external wall.

Fig. 4. The location and side view of the office building.

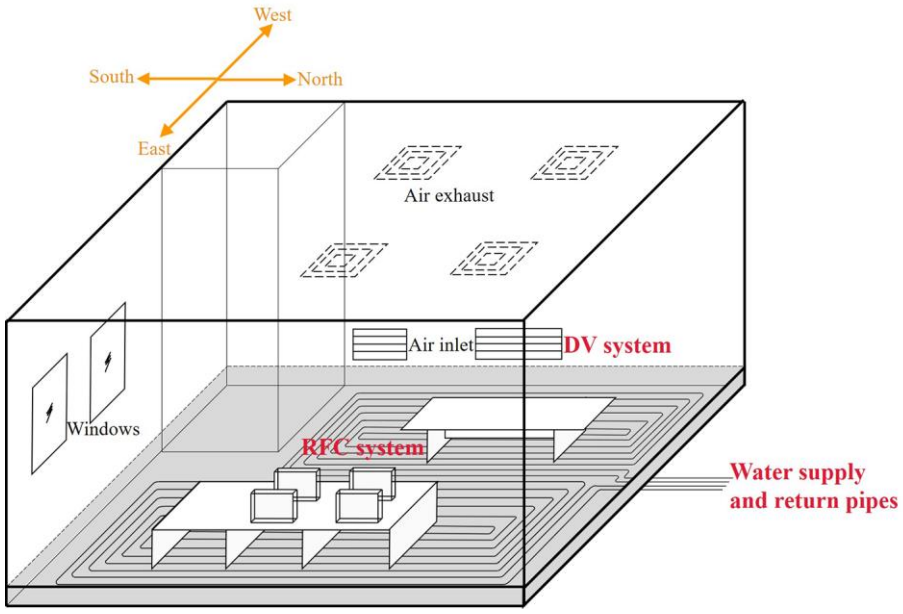

Fig. 5. Schematic diagram of the RFC and DV systems.

As shown in Fig. 5, the schematic diagram of the integrated RFC and DV system is presented. The following boundary conditions were set according to the actual operational conditions of the composite system in the experimental office building [18,43]. The supply airflow rate, supply air temperature, chilled water flow rate, and supply water temperature were set to 155 m^3/h, 20 °C, 0.153 kg/s, and 18 °C, respectively, according to the design cooling load of 0.05 kW/m^2 of the office building. The internal heat source covered 11 W/m^2, 20 W/m^2, and 4 m^2/person for lighting, equipment, and occupants, respectively. The activity level of the occupants was 134 W/person, the clothing factor was 0.5 clo, and the metabolic rate was 1.2 met. The circulating water extracted cooling energy from an underground heat exchanger and was supplied at a stable temperature to the radiant floor terminal. The fresh air supplied by the DV system cooled down and dehumidified the indoor air during the starting and the operation periods.

2.4 Simulation implementation

The simulation process for different cases is shown in Fig. 6. jEPlus was used to set the values of the

operational parameters and the heat source levels of the RFC and ventilation system within a reasonable range. The outdoor temperature and humidity parameters were changed in the EPW file included in TRNSYS. The simulations were conducted after setting the indoor and outdoor parameters and the operational parameters, and the output results were obtained. The data were processed to determine the effect of different operational parameters. Simultaneously, the cooling load shared by the RFC and ventilation systems was obtained by minimizing the energy consumption within the comfort zone to create the S_v/S_R adjustment strategy.

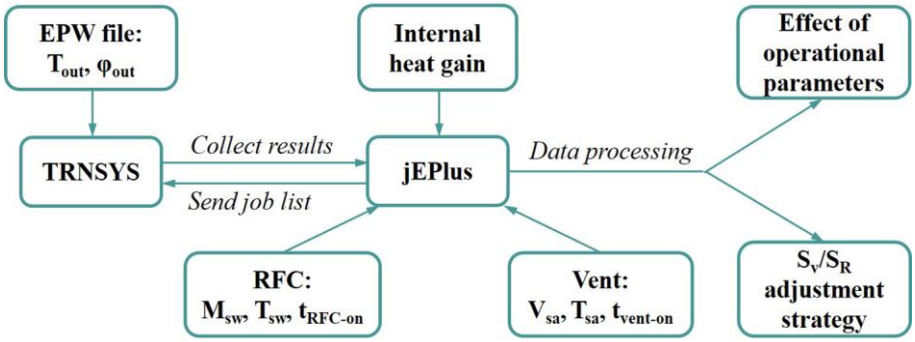

Fig. 6. Simulation framework of this study.

2.5 Description of the PMV-based control

2.5.1 PMV for thermal comfort assessment

The PMV model [44] is the most frequently used and best-understood model for quantitative thermal comfort analysis. The PMV is defined as a function of six thermal variables related to indoor air conditions and human behaviors, including air temperature, air humidity, air velocity, mean radiant temperature, clothing insulation level, and human activity. The PMV index represents the thermal sensation of the majority of occupants exposed to the same environment. Generally, the air temperature and the mean radiant temperature are close to the neutral point in practical engineering applications of the radiant terminal; thus, the PMV model can be used for predicting the occupant's thermal sensation [45]. Therefore, the PMV was used in this study to determine the thermal comfort constraint, and PMV-based prediction was the central part of the proposed control.

2.5.2 The PMV-based control framework

As shown in Fig. 7, the experimental data and physical characteristics were utilized to establish the building energy model and obtain the PMV and energy consumption. The collaborative control of the RFC system and ventilation system was implemented.

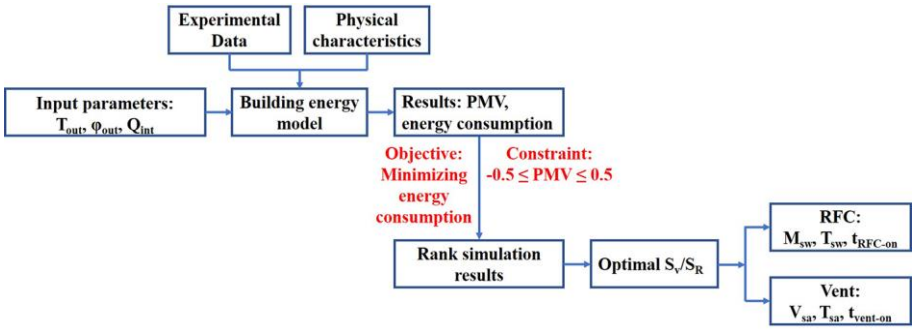

Fig. 7. The PMV-based control workflow.

The outdoor air temperature, air humidity, and internal heat gain related to occupant schedule were input into the building energy model, and the output was the PMV and energy consumption. The PMV was calculated according to the standard of ASHRAE 55-2013 [46]. The system's energy consumption includes the energy consumption of the RFC system and ventilation system. The RFC system utilizes underground circulating water to provide free cooling. Thus, only the circulation pumps consume power, which is calculated by Eq. (3). In contrast,

the ventilation system consumes energy for operating the fan and cooling. Its power is calculated using Eqs. (4)−(7).

$$E_{pump} = \int \frac{\rho_{sw} g H V_{sw}}{\eta_{pump}}\, dt \tag{3}$$

where E_{pump} is the energy consumption of the water circulating pump, kWh; ρ_{sw} is the density of the supply water, kg/m^3; g is the acceleration of gravity, m/s^2; H is the water circulating pump head, m; V_{sw} is the supply water volume flow rate, m^3/h; η_{pump} is the water circulating pump efficiency.

$$E_{fan} = \int \frac{\Delta P \times V_{sa}}{1000 \eta_{fan}}\, dt \tag{4}$$

where E_{fan} is the energy consumption of the fan, kWh; ΔP is the pressure rise through the supply fan, Pa; V_{sa} is the supply water volume flow rate, m^3/s; η_{fan} is the fan efficiency.

$$Q_{cl,sens} = \int m_{sa} \cdot c_p (T_{out} - T_{set})\, dt \tag{5}$$

$$Q_{cl,dehum} = \int \rho_a V_{sa} \cdot c_p \left(T_{out} - T_{out,dew}\right) + \Delta h_V \cdot \rho_a V_{sa} (\omega_{out} - \omega_{max})\, dt \tag{6}$$

$$Q_{ht,reheat} = \int m_{sa} \cdot c_p (T_{set} - T_{out,dew})\, dt \tag{7}$$

where $Q_{cl,sens}$ is the sensible energy to cool down the air to the set point temperature, kWh; V_{sa} is the supply air volume flow rate, kg/h; c_p is the specific heat, J/(kg•K); T_{out} is the outdoor air temperature, °C; $Q_{cl,dehum}$ is the latent energy to dehumidify the air to the setpoint humidity, kWh; ρ_a is the density of the supply air, kg/m^3; T_{set} is the setpoint temperature, °C; $T_{out,dew}$ is the dewpoint temperature of the outdoor air, °C; Δh_v is evaporation enthalpy, J/kg; ω_{out} is the outdoor air humidity ratio, g/kg; ω_{max} is the maximum humidity, g/kg; $Q_{ht,reheat}$ is the sensible energy to reheat the air, kWh.

Based on the indoor thermal comfort constraints and the objective to minimize energy consumption, the simulation results were ranked to determine the cooling energy supply of the two systems with optimal S_v/S_R using the theoretical Eqs. (8)−(9)[22,47]. Suitable adjustments were made to each operational parameter. In the next control time step, a new optimal control problem was formulated and solved based on the optimal output and the updated indoor and outdoor parameters.

$$Q_{RFC} = \mathrm{A} \int h_t (T_{op} - T_f)\, dt \tag{8}$$

where Q_{RFC} is the total cooling energy provided by the RFC system during a limited period, kWh; A is the floor surface area, m^2; h_t is total heat transfer coefficient, W/(m^2·K); T_{op} is the operative temperature, °C; T_f is the floor surface temperature, °C.

$$Q_{vent.} = \rho_a c_p \int V_{sa} (T_{in} - T_{sa})\, dt \tag{9}$$

where $Q_{vent.}$ is the total sensible cooling energy provided by the ventilation system during a limited period, kWh; V_{sa} is the supply air volume flow rate, m^3/s; T_{in} is the indoor air temperature, °C; T_{sa} is the supply air temperature, °C.

2.6 Simulation conditions

Table 2 lists the settings of various initial indoor conditions, outdoor weather conditions and internal heat gain in the starting stage and operation stage. Jinan city in northern China was selected. It is located in a cold climate zone where summers are hot and rainy and last for 105~120 days. Outdoor temperature and humidity parameters were derived from a typical meteorological year data of Jinan. Table 2 listed settings of indoor and outdoor conditions. Q in Table 2 represents a heat gain of 11 W/m^2, 20 W/m^2, and 4 m^2/person for lighting, equipment, and occupants, respectively [48]. The outdoor temperature and humidity over time for different outdoor weather conditions and the internal heat source schedule are shown in Fig.8. The various outdoor weather conditions were created by setting a constant difference between different outdoor temperature and different relative humidity curves. The periods marked in the figures were used for the simulation, with a time step of one minute.

Table 2

Settings of indoor and outdoor conditions.

Indoor and outdoor conditions	Starting stage	Operation stage
T_{ini} (°C)	28, 30	26.5
φ_{ini} (%)	75, 85	65
$T_{out\text{-}max}$ (°C)	30, 32	30, 32, 34, 36
$\varphi_{out\text{-}max}$ (%)	80, 90	70, 80, 90
Q_{int} (kW)	——	0.5Q, Q, 2Q

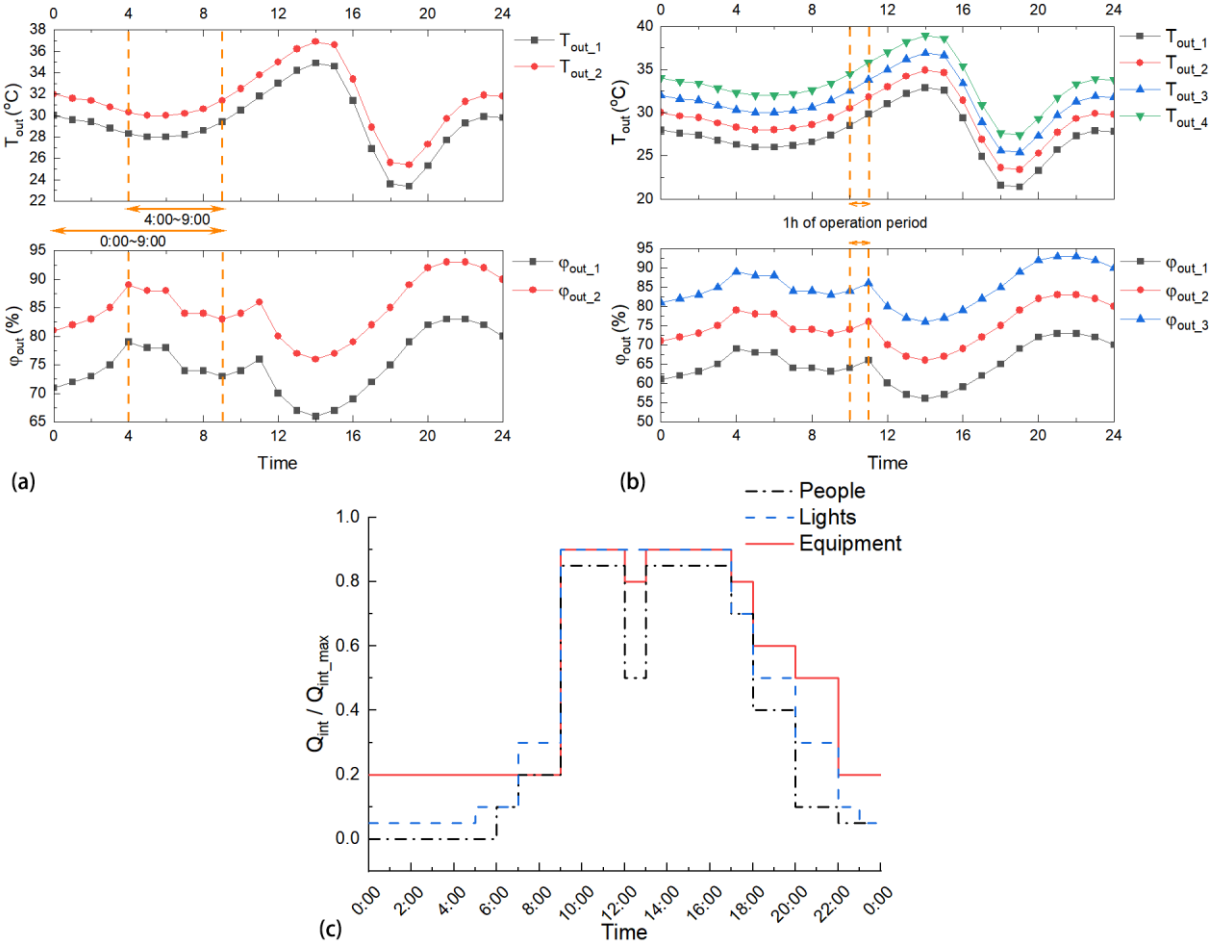

Fig. 8. Outdoor and indoor conditions: (a) T_{out} and φ_{out} in the starting stage, (b) T_{out} and φ_{out} in the operation stage, and (c) internal heat source schedule.

The operational parameters settings of the RFC and ventilation system based on practical operations [49] are listed in Table 3. A total of 4820 cases were simulated, requiring a computing time of about 50 h.

Table 3

Operational parameter settings.

Operational parameters		Starting stage	Operation stage
RFC	M_{sw} (kg/s)	T_{ini}=28 °C: 0.097, 0.110, 0.125 T_{ini}=30 °C: 0.153, 0.166, 0.180	0.097, 0.110, 0.125
	T_{sw} (°C)	18, 20, 22	18, 20, 22
	$t_{RFC\text{-}on}$	T_{ini}=28 °C: 0:00, 1:00, 2:00 T_{ini}=30 °C: 4:00, 5:00, 6:00	——
Ventilation	T_{sa} (°C)	18, 20, 22	18, 20, 22
	V_{sa} (m^3/h)	First stage[a]: φ_{ini}=75% required 50, φ_{ini}=85% required 100	78, 116, 155, 194

	Second stage[b]: 78, 116, 155, 194	
$t_{vent.-on}$	First stage[a]: φ_{ini}=75% required at the same time as t_{RFC-on}, φ_{ini}=85% required 1 hour earlier than t_{RFC-on} Second stage[b]: 6:00, 7:00, 8:00	——

[a]Note: Start time of first ventilation to prevent condensation

[b]Note: Start time of second ventilation to meet standard humidity level

2.7 Simulation validation

An experiment was carried out in a south-facing room on the fifth floor of an office building in Jinan from August to September 2020 [43,50]. The combined RFC system and DV system was investigated in the experiment. The detailed model information was provided in Section 2.3. The outdoor weather conditions are shown in Fig. 9. T_{out} was essentially below 35 °C, and φ_{out} mostly exceeded 90% from Aug. 13 to 17.

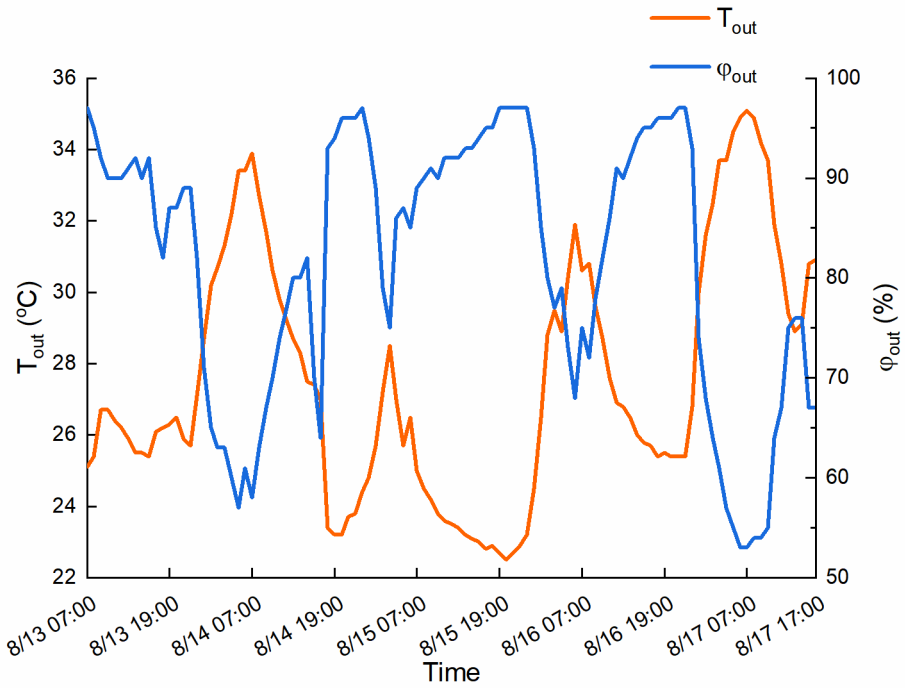

Fig. 9. Outdoor weather data during the experimental period from Aug. 13 to Aug. 17 in 2020.

The schematic diagram of the field test in the office building are presented in Fig. 10. The T_{in} and φ_{in} were obtained from temperature and humidity sensors at the height of 1.1 m in the center of the room. Fig. 11 shows the simulated and measured power consumption, T_{in} and φ_{in} of the composite system obtained from Aug. 13 to 17. As shown in Fig. 11a, there was high similarity between the measured and simulated power consumption. The calculated mean bias error (MBE) and root mean square error (RMSE) [51] were -0.01 and 0.1, respectively. The measured and simulated values of T_{in} and φ_{in} from Aug. 13 to 17 were also compared to verify the model accuracy. As shown in Fig. 11b and Fig. 11c, the measured T_{in} and φ_{in} values were in good agreement with the simulated values. Correspondingly, the MBE and RMSE of the T_{in} (φ_{in}) data were 0.22 and 0.46 (0.7 and 3.43), respectively.

Fig. 10. The schematic diagram of the field test in the office building [43].

Moreover, the coefficient of variation of the root mean square error (CVRMSE) and normalized mean bias error (NMBE) calculated by Eq. (10) and Eq. (11) were also used to validate the accuracy of the simulation model [52]. The calculated NMBE was -0.07 % and the CVRMSE was 0.7 %. These values should satisfy the standard requirements: -5 % ≤ NMBE ≤ 5 %, and CVRMSE ≤ 15 % [52]. Therefore, the validation showed that the model had sufficiently high accuracy.

$$CVRMSE = \frac{\left[\sum_{i=1}^{n}(y_i-\hat{y}_i)^2/(n-p)\right]^{1/2}}{\bar{y}} \times 100 \tag{10}$$

$$NMBE = \frac{\sum_{i=1}^{n}(y_i-\hat{y}_i)}{(n-p)\times\bar{y}} \times 100 \tag{11}$$

where $\hat{y}_i$ denotes the predicted data, y_i is the calibrated data, and $\bar{y}$ is the average value with p = 1.

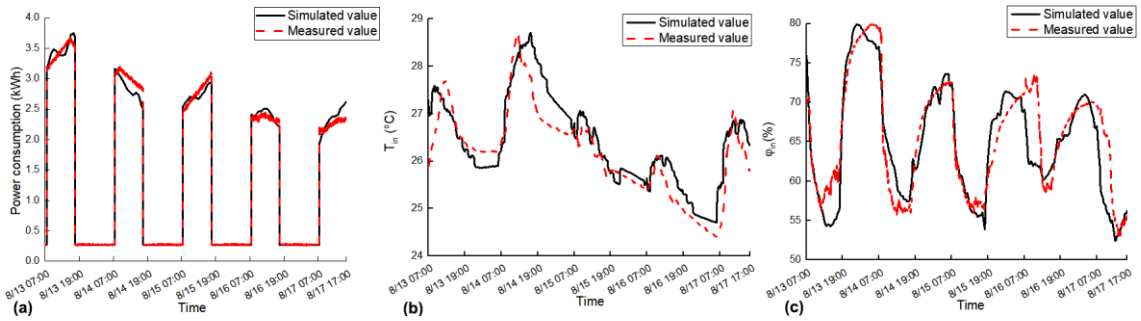

Fig. 11. Comparison of the simulated and measured results. (a) power consumption, (b) T_{in}, and (c) φ_{in}.

3 Results

3.1 Starting stage

3.1.1 The effect of the outdoor weather and initial indoor conditions on Q_{total}

As shown in Fig. 12, the Q_{total} under different outdoor weather conditions and two initial indoor conditions with the S_v/S_R range of 0.03~0.16 and 0.03~0.1 is presented, respectively. The results were divided into three parts: the first, middle two, and last quarters. The S_v/S_R value represents the proportion of the total sensible heat removed by the RFC system to the total sensible heat removed by the ventilation system in the starting stage. Q_{total} of the composite system showed an increasing trend with a decrease in the S_v/S_R. As the T_{ini} increased from 28 °C to 30 °C, i.e., an increase in the indoor load, Q_{total} increased significantly, and the maximum value of S_v/S_R decreased. The results indicated that the increase in Q_{total} mainly depended on improving the cooling capacity of the radiant floor system; thus, the RFC system should be precooled to lower the T_{in}. In addition, as the φ_{ini} increased, Q_{total} increased significantly. The results show that the initial indoor conditions had a greater impact on

the Q_{total} than the outdoor weather conditions and were the dominant factor affecting the starting control of the composite system.

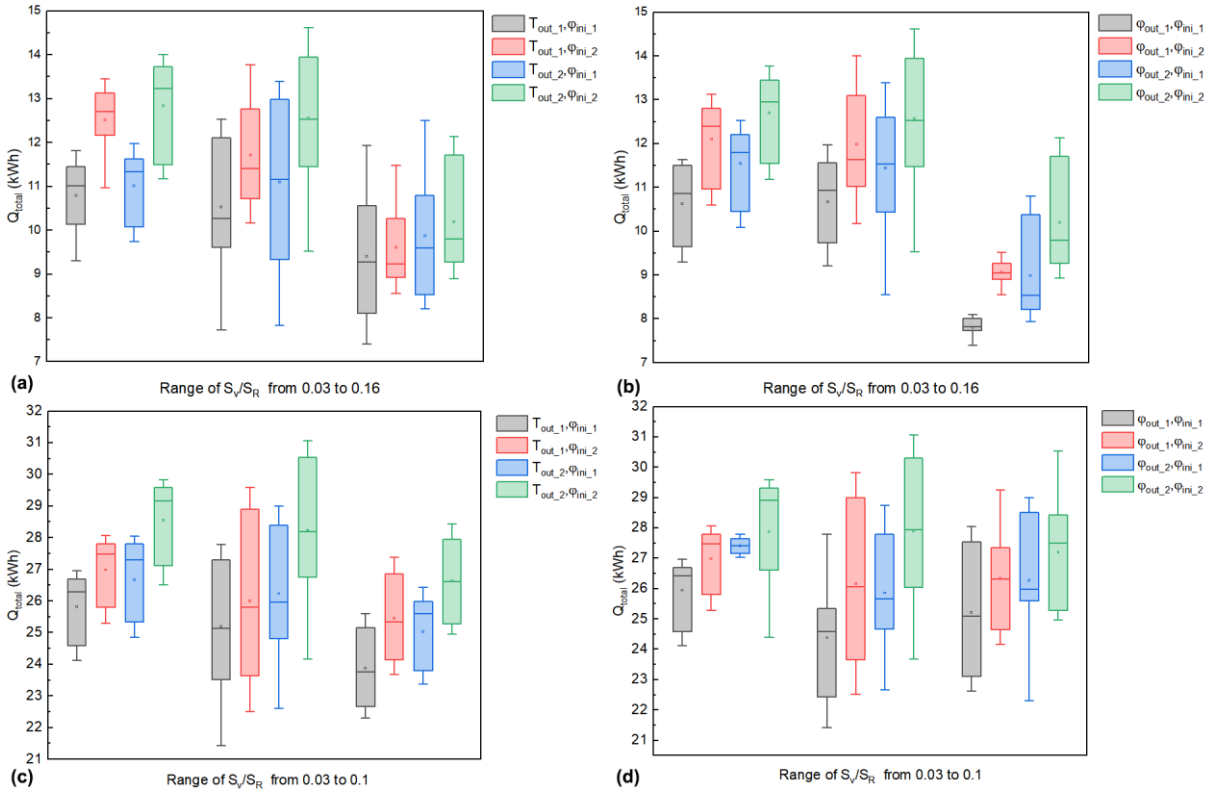

Fig. 12. Q_{total} within the S_v/S_R range under different initial indoor and outdoor weather conditions: (a) effect of the T_{out} at T_{ini} of 28 °C, (b) effect of the φ_{out} at T_{ini} of 28 °C, (c) effect of the T_{out} at T_{ini} of 30 °C, and (d) effect of the φ_{out} at T_{ini} of 30 °C.

3.1.2 The correlation between S_v/S_R, PMV, and energy consumption

The correlations between S_v/S_R, the final PMV at the end of the starting stage, and total energy consumption at different T_{ini} (28 °C and 30 °C) are shown in Fig. 13. Since the RFC system was started 3~6 h earlier at the T_{ini} of 30 °C than at 28 °C, in addition to a large increase in V_{sa}, the total energy consumption was significantly higher at the T_{ini} of 30 °C to achieve the same comfort level. The maximum energy consumption was 14.2 kWh at 28 °C and 21.85 kWh at 30 °C. Due to the much longer cooling time of the RFC system than the ventilation system in the starting stage, the RFC system provided significantly more cooling energy, resulting in a lower S_v/S_R in different initial indoor conditions. The maximum S_v/S_R value was close to 0.3 (0.18) at 28 °C (30 °C). It was concluded that the energy consumption growth was related to the S_v/S_R increase and the decrease of the final PMV value. Therefore, a lower S_v/S_R should be used to achieve energy consumption reduction while ensuring a final PMV value within the comfort zone of -0.5 to 0.5 [46].

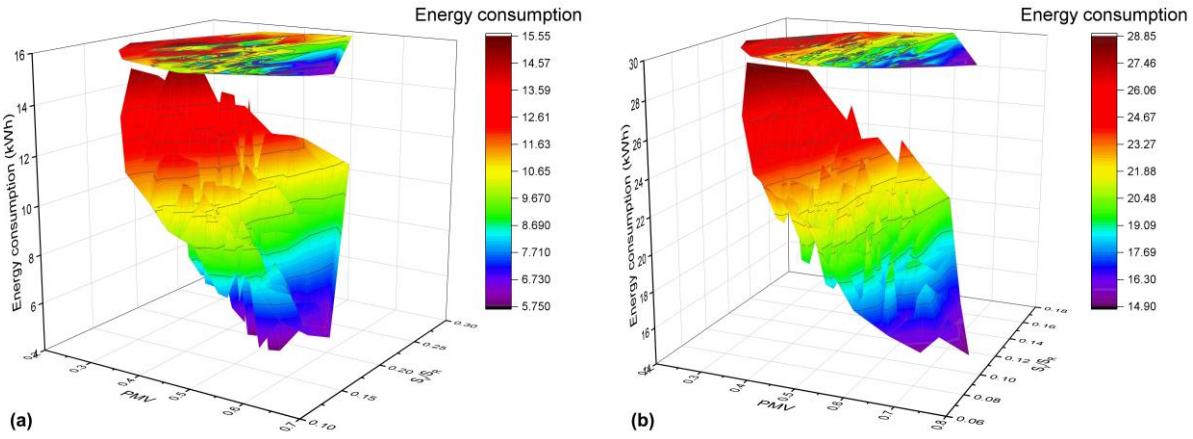

Fig. 13. The correlation between S_v/S_R, PMV, and energy consumption at different T_{ini}: (a) T_{ini} of 28 °C and (b) T_{ini} of 30 °C.

3.1.3 Control measures to prevent condensation and variation of the latent heat load

The control measures for the ventilation system to prevent condensation under different φ_{ini} conditions is shown in Fig. 14. The pre-dehumidification time of the ventilation system ($t_{pre\text{-}dehum}$) started 1 hour earlier than the activation time of the RFC system (4:00, 5:00, 6:00) at a φ_{ini} of 85%. The energy consumption of the ventilation system and the duration from $t_{pre\text{-}dehum}$ to the time when T_f is higher than T_{dp} (τ) for V_{sa} values of 38 m^3/h, 78 m^3/h, and 116 m^3/h are shown in Fig. 14a. The energy consumption rose stably, and τ decreased rapidly with an increase in V_{sa} from 38 m^3/h to 78 m^3/h. τ decreased slowly as V_{sa} increased from 78 m^3/h to 116 m^3/h. The V_{sa} of 78 m^3/h was selected for all the φ_{ini} of 85% to prevent condensation and achieve a trade-off between energy consumption and τ. Fig. 14b shows the temperature difference between T_f and T_{dp} (Δt) with and without an air supply at a φ_{ini} of 75%. When the RFC system operated without an air supply, T_f quickly decreased below T_{dp}. When the same starting time was used for the RFC system and the ventilation system with a V_{sa} of 38 m^3/h, T_f was always higher than T_{dp} and Δt gradually increased, preventing condensation on the radiant surface. Therefore, the radiant cooling system must be started at the same time as the ventilation system with a V_{sa} of 38 m^3/h to prevent condensation risks. This control measure to prevent condensation is applicable to the φ_{ini} of 75%.

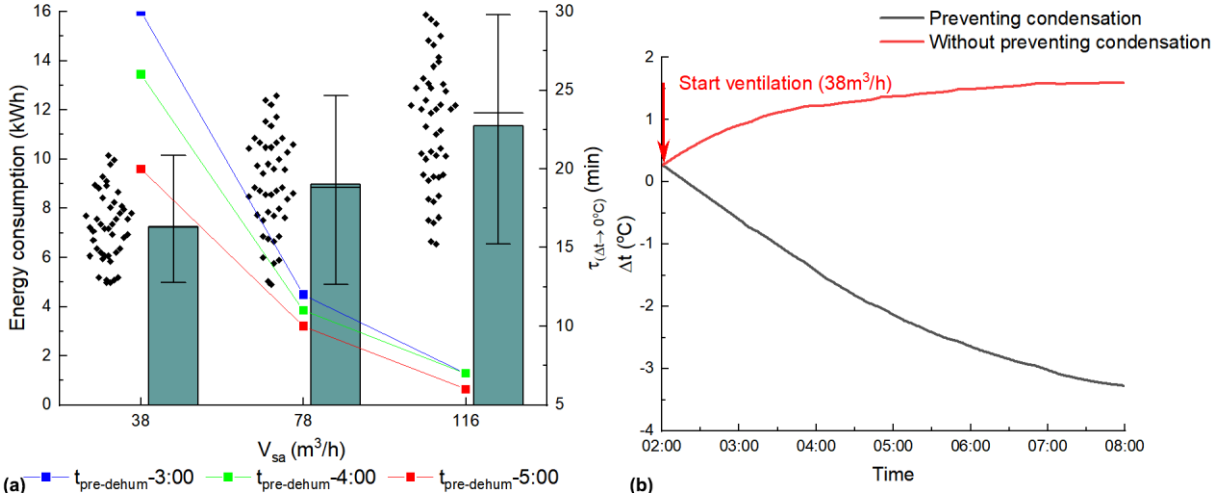

Fig.14. Control measures to prevent condensation under different φ_{ini} conditions: (a) φ_{ini} of 85% and (b) φ_{ini} of 75%.

Fig. 15 depicts the effects of different V_{sa} conditions on the latent heat load and the proportion of the latent heat load to the total cooling load during the starting stage. Due to dehumidification by the ventilation system, the indoor moisture load decreased, leading to a reduction in the moisture exchange between the ventilation system

and the indoor environment and a decrease in the latent heat load removed by the ventilation system; thus, the total cooling load decreased. Due to continuous sensible heat transfer from the outdoor to the indoor environment with an increase in T_{out}, the proportion of the sensible heat load removed by the composite system increased, whereas the proportion of the latent heat load decreased, shifting the focus of the load handling task of the composite system. A comparison of the latent heat load and the proportion of the latent heat load for the three V_{sa} indicated that a larger V_{sa} provided a higher dehumidification rate and a higher rate of decrease in the moisture load.

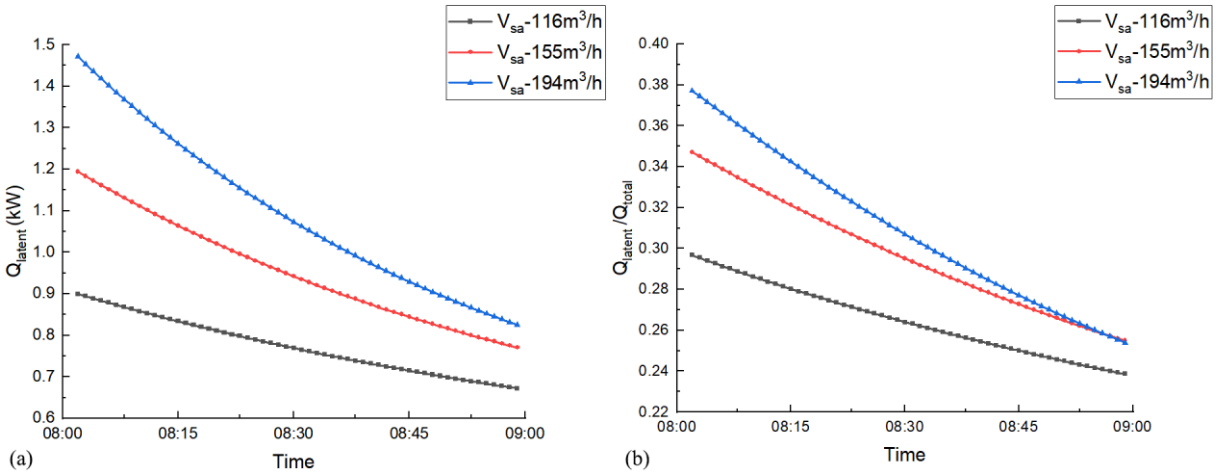

Fig. 15. The effects of different V_{sa} on the (a) latent heat load and (b) proportion of the latent heat load to the total cooling load.

3.1.4 The effect of different operational parameters on PMV and energy consumption

The effects of $t_{RFC\text{-}on}$, M_{sw}, and V_{sa} during the second ventilation step on the final PMV and energy consumption in the starting stage under different T_{ini} conditions are illustrated in Fig. 16. The RFC system was activated earlier at the T_{ini} of 30 °C than at 28 °C, and the M_{sw} and V_{sa} were higher; therefore, the total energy consumption was higher at 30 °C than at 28 °C. It was noted that the PMV values corresponding to the first value of each parameter was higher than 0.5, leading to infeasible solutions. The optimization space can be simplified by detecting infeasible values to improve the optimization efficiency. Precooling of the RFC system was used to provide indoor cooling during the start-up period; thus, the $t_{RFC\text{-}on}$ and M_{sa} had notable effects on the total energy consumption of the composite system and the final PMV. The ventilation system was responsible for dehumidification to meet the standard humidity level. A change in the V_{sa} at a given T_{sa} and $t_{vent.\text{-}on}$ directly affected φ_{in}, which significantly impacted the indoor thermal comfort. Therefore, the ranking of the three parameters regarding their effects on the final PMV was $V_{sa} > t_{RFC\text{-}on} > M_{sw}$. However, since the ventilation control was divided into two periods to supply air in the starting stage, and the second ventilation accounted for a small proportion, a change in the V_{sa} during the second ventilation step had a relatively small impact on total energy consumption. Therefore, the ranking of the three parameters regarding their effects on energy consumption was $t_{RFC\text{-}on} > V_{sa} > M_{sw}$. Based on the effects of the three parameters, suitable adjustments of the operation parameters could be made to minimize energy consumption and satisfy the total cooling energy demand.

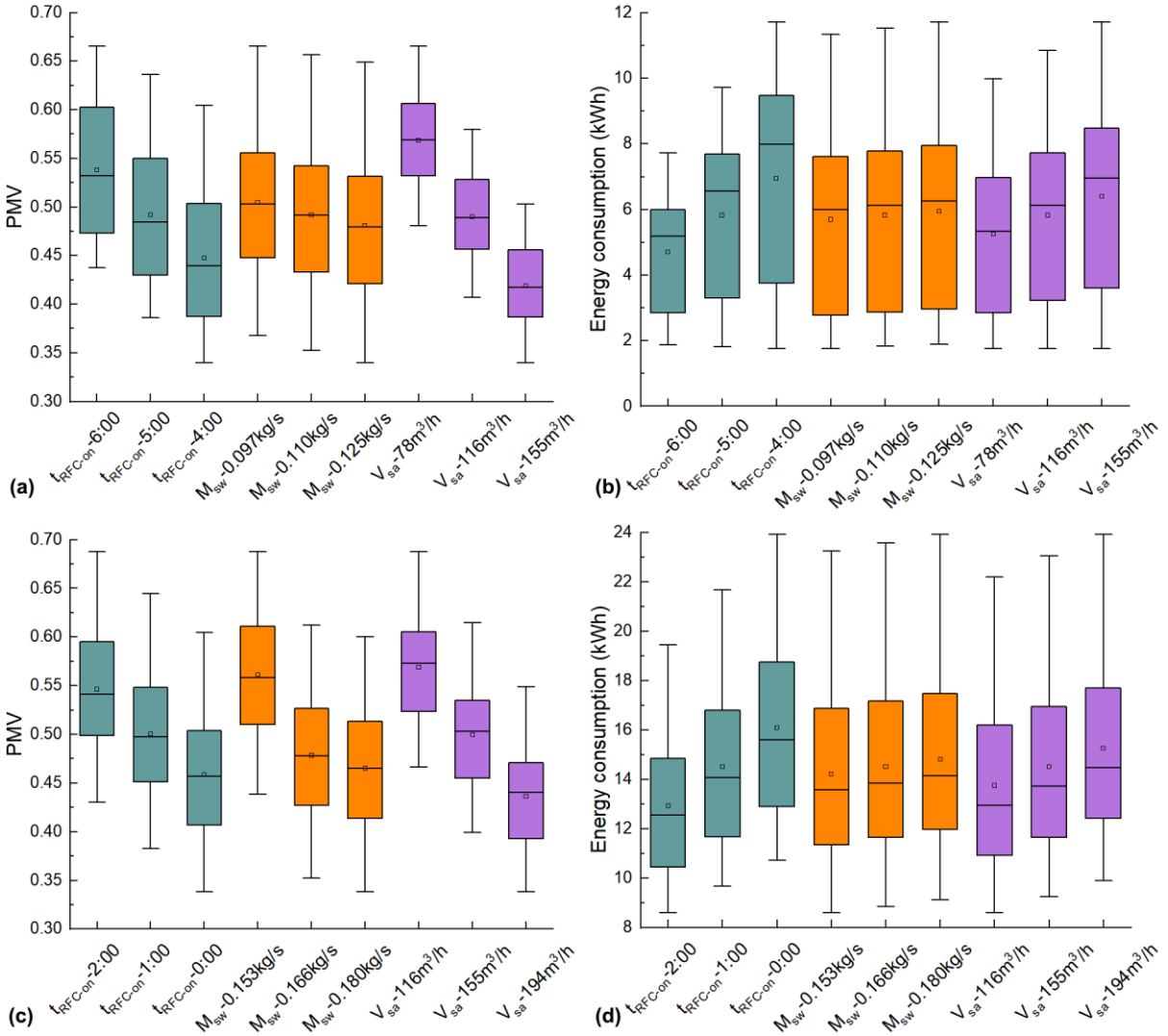

Fig. 16. The effect of t_{RFC-on}, M_{sw}, and V_{sa} on PMV and energy consumption under different T_{ini} conditions: (a) effect on PMV at T_{ini} of 28 °C, (b) effect on energy consumption at T_{ini} of 28 °C, (c) effect on PMV at T_{ini} of 30 °C, and (d) effect on energy consumption at T_{ini} of 30 °C.

3.2 Operation stage

3.2.1 The effect of the outdoor weather conditions and internal heat gain on Q_{total}

Fig. 17 shows Q_{total} under different outdoor weather conditions and internal heat gains in the S_V/S_R value range of 0.03~0.25, which was divided into the first, the middle two, and the last quarter. The total sensible heat removed by the RFC system and that removed by the ventilation system in the operation stage were calculated to obtain S_V/S_R. Q_{total} increased with an increase in the S_V/S_R, indicating that enhancing Q_{total} primarily depended on increasing the cooling capacity of the ventilation system. An increase in the internal heat gain had a more significant effect on Q_{total} (an increase of 0.2~0.5 kWh in Q_{total}) than an increase in the T_{out} and φ_{out}. The reason was that heat and moisture transfer from outdoors to indoors was reduced due to the thermal resistance of the building envelope. An increase in the internal heat gain caused an increase in indoor heat and moisture loads and had a direct effect on the indoor thermal environment. Therefore, it is necessary to focus on addressing the internal heat gain by increasing the cooling energy supply of the composite system.

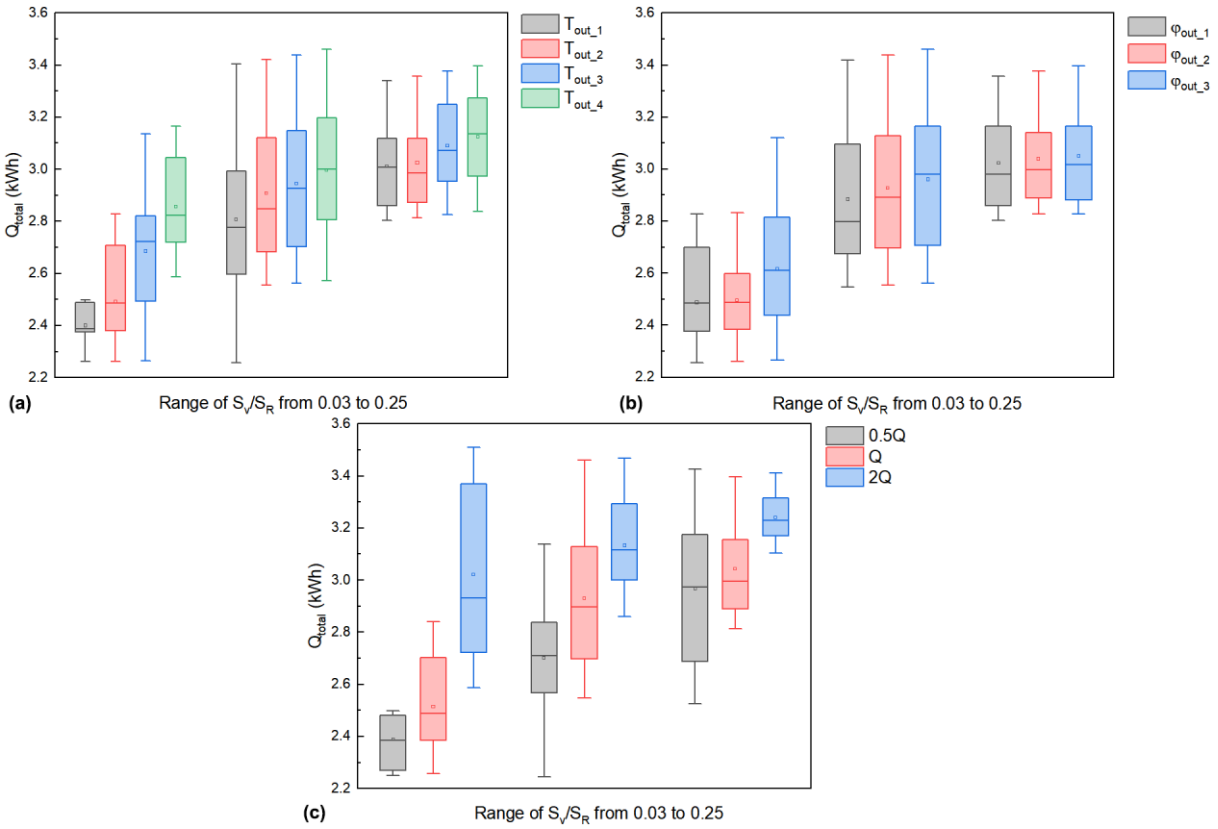

Fig. 17. Q_{total} within the S_v/S_R range under different T_{out}, φ_{out}, and Q_{int} conditions: (a) effect of T_{out}, (b) effect of φ_{out}, and (d) effect of Q_{int}.

3.2.2 The S_v/S_R, Q_{total}, and energy consumption at different PMV proportions

Fig. 18 shows the S_v/S_R, Q_{total}, and energy consumption with an increase in the PMV proportion per minute within the comfort zone during a 1 h operation period. The S_v/S_R increased as the PMV proportion increased. Although the RFC system removed the majority of the sensible heat load, the proportion of sensible heat load removed by the ventilation system must be increased due to the high cooling efficiency of the ventilation system to enhance the cooling capacity of the composite system. An effective solution is to efficiently deal with the indoor heat and moisture loads to achieve a higher thermal comfort level. However, the S_v/S_R decreased when the PMV proportion slightly increased, indicating that the cooling energy by the RFC system should be increased if the PMV proportion was close to 100%. The energy consumption level was related to Q_{total} and the S_v/S_R. A higher S_v/S_R resulted in higher energy consumption with a similar Q_{total}. It could be concluded that the S_v/S_R must be increased to prevent a large PMV deviation from the comfort zone. In contrast, the S_v/S_R could be adjusted by the self-regulation control of the RFC system if the PMV was close to the comfort zone. Based on indoor thermal comfort constraints, the S_v/S_R should be minimized to reduce energy consumption.

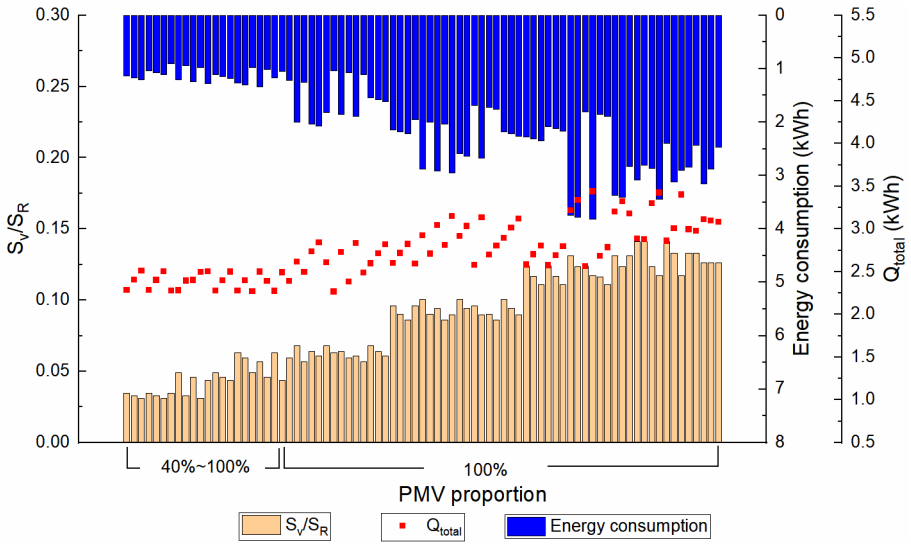

Fig. 18. The S_v/S_R, Q_{total}, and energy consumption at different PMV proportions.

3.2.3 The effect of different operational parameters on PMV and energy consumption

Fig. 19 illustrates the effects of M_{sw}, T_{sa}, and V_{sa} on the PMV and energy consumption in the operation stage. Due to the thermal inertia of the radiant structure, a change in the M_{sw} had a negligible effect on the indoor thermal environment. By comparison, it is more efficient to adjust T_{sa} and V_{sa} to improve indoor thermal comfort. The ranking of the three parameters regarding their effects on the PMV and energy consumption was V_{sa} > T_{sa} > M_{sw}. Therefore, the cooling capacity of the ventilation system should be adjusted to ensure acceptable indoor thermal comfort in the operation stage. Based on the effect of the three parameters, suitable adjustments to the operational parameters should be made to minimize energy consumption and satisfy the total cooling energy demand.

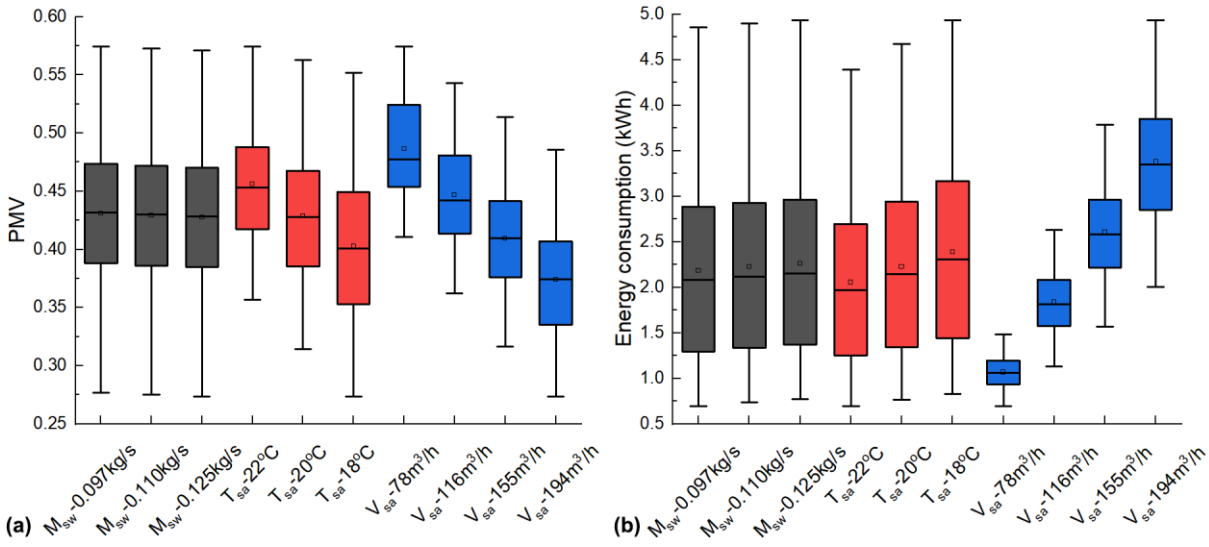

Fig. 19. The effect of M_{sw}, T_{sa}, and V_{sa} on the (a) PMV and (b) energy consumption.

4. Proposed control strategy

4.1 Collaborative control strategy

The collaborative control strategy was developed considering the energy consumption and cooling performance differences between the radiant and air systems. Unlike air systems, radiant systems utilize water as the thermal medium because it has a much higher thermal capacity than air, resulting in less energy consumption with relatively low pumping energy. Moreover, the indoor cooling load of an air system is approximately equal to

the heat extraction by the mechanical system. In contrast, the heat load removed from a room at the radiant surface of the RFC system is quite different from that removed by the hydronic loop, indicating a decrease in and delay of the cooling energy supply [53]. As a result, the cooling capacity of radiant systems is limited when dealing with thermal comfort reduction due to increased heat and moisture loads. When the thermal comfort level can be controlled by the radiant system, using the self-regulating effect of the radiant surface temperature and adjusting the operational parameters can modify the heat exchange between the radiant structure and the indoor thermal environment. If the radiant system cannot provide an acceptable thermal comfort level, the cooling capacity of the air system must be improved.

The collaborative control strategy of the composite system is illustrated in Fig. 20. The main feature is that the collaborative controls are determined by the final PMV in the starting stage and the PMV proportion in the operation stage. Therefore, the cooling energy supply matches the load demand, improving the control accuracy and efficiency. The initial operational parameters of the RFC system and ventilation system were determined based on the current indoor loads and outdoor weather conditions. The collaborative control strategy was implemented for the starting stage and the operation stage.

In the starting stage, when T_s-$T_{dp} \leq 0$ °C , the ventilation system was started while the RFC system was shut down to prevent condensation. When T_s-$T_{dp} > 0$ °C and there was no condensation risk, the S_v/S_R was adjusted based on the final PMV. If the final PMV ≤ 0.5, which met the comfort standard, the ventilation system could be turned off. If the final PMV > 0.5, the cooling energy supply of the RFC system and the ventilation system were increased. In the operation stage, if the PMV proportion = 1, the ventilation system provided a minimum amount of fresh air to ensure good indoor air quality, resulting in energy savings. If the PMV proportion <1, it was required to increase the cooling energy supply of the ventilation system combined with the self-regulation control of the RFC system.

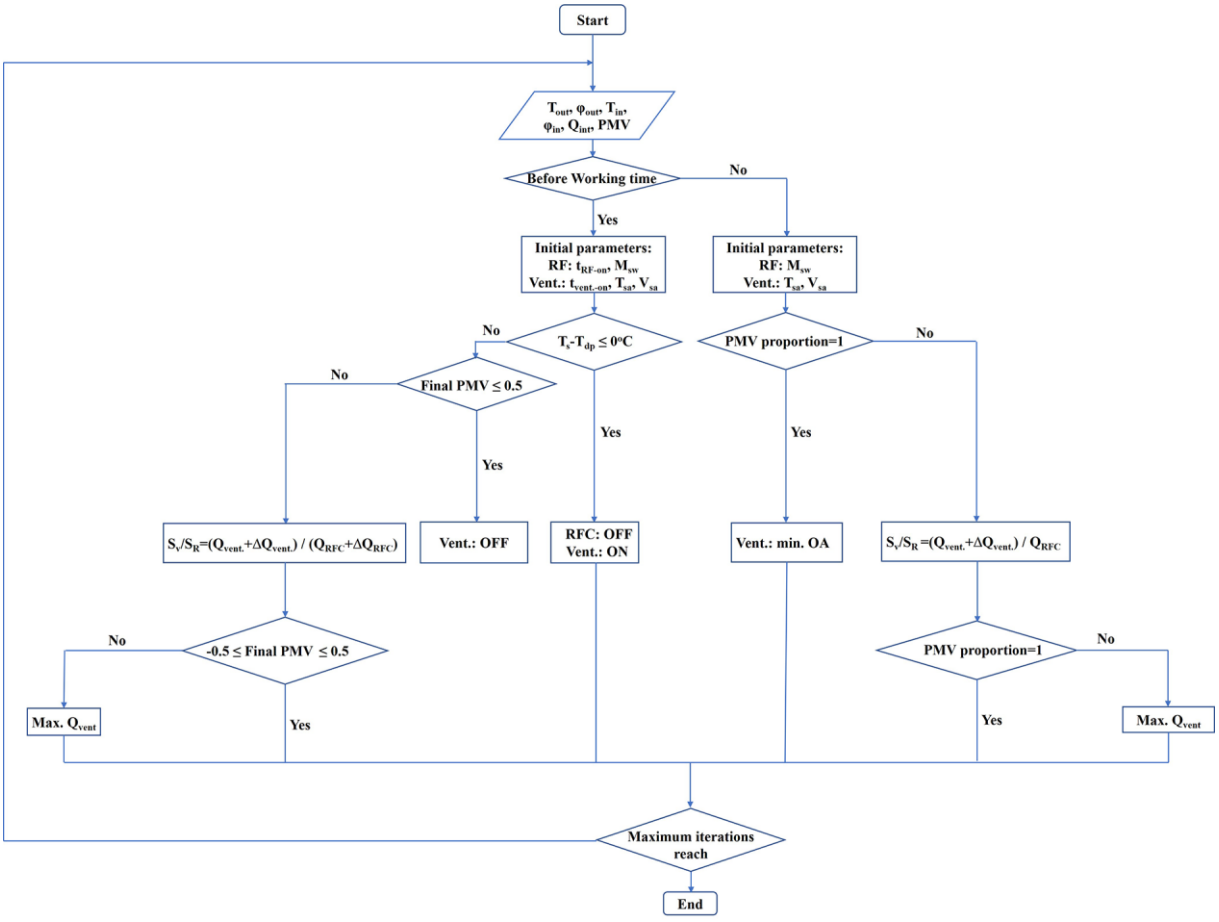

Fig. 20. Proposed collaborative control strategy.

4.2 Comparison of different control strategies

As shown in Fig. 21, the outdoor weather conditions for the comparison of different control strategies from Jul. 2 to Jul. 6 is depicted. The comparison of the energy consumption between the common control strategy and the proposed collaborative control strategy is shown in Fig. 22. The PMV index was within -0.5~0.5 for the two control strategies, and the proposed collaborative control strategy achieved total energy savings of 22.4%, as shown in Table 4. The common control strategy used an ON/OFF control of the RFC system with a fixed operation schedule from 4:00~17:00, and the RFC system operated with a constant M_{sw}. The air supply of the ventilation system was determined by the moisture load to be removed, and the relationship between T_f and T_{dp} before 9:00 and after 9:00 was based on the indoor temperature and humidity set point at 26 °C and 65%, respectively, which is the basic control applied to the radiant cooling systems.

The two control strategies provided a comparable operational performance of the system with relatively small energy consumption differences because there was little internal heat gain, and dehumidification was the main task without a thermal comfort requirement for the cooling system before the end of the starting stage. In contrast, in response to dynamic changes in the indoor thermal environment during the operation stage, the RFC system operated until the end of the operation schedule in the common control strategy, wasting cooling energy. In contrast, the proposed collaborative control strategy based on the PMV-based prediction adapted better to the variable internal heat gain; thus, the hysteresis of the cooling energy supply and demand was overcome, and fluctuations in energy consumption were attenuated. Therefore, the collaborative control strategy showed significantly higher energy savings. The daily energy savings were 23.9%, 26.2%, 21.5%, 21%, and 21.3% on Jul. 2, 3, 4, 5, and 6, respectively.

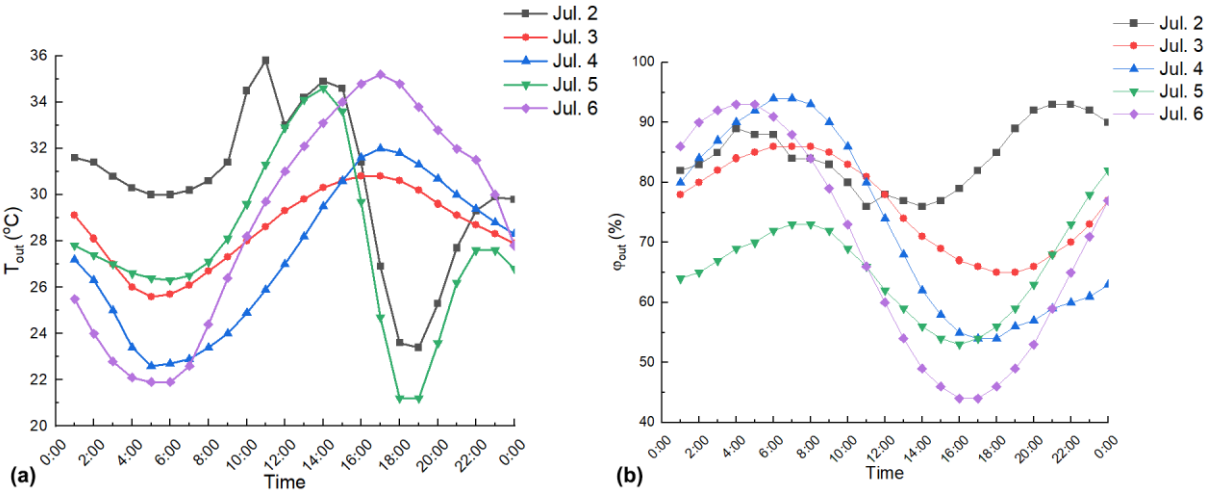

Fig. 21. Outdoor weather conditions from Jul.2 to Jul. 6: (a) T_{out} and (b) φ_{out}.

Table 4

Total energy consumption of different control strategies.

	Energy consumption (kWh)	Energy saving (%)
Common	103.47	-
Proposed	80.32	22.4

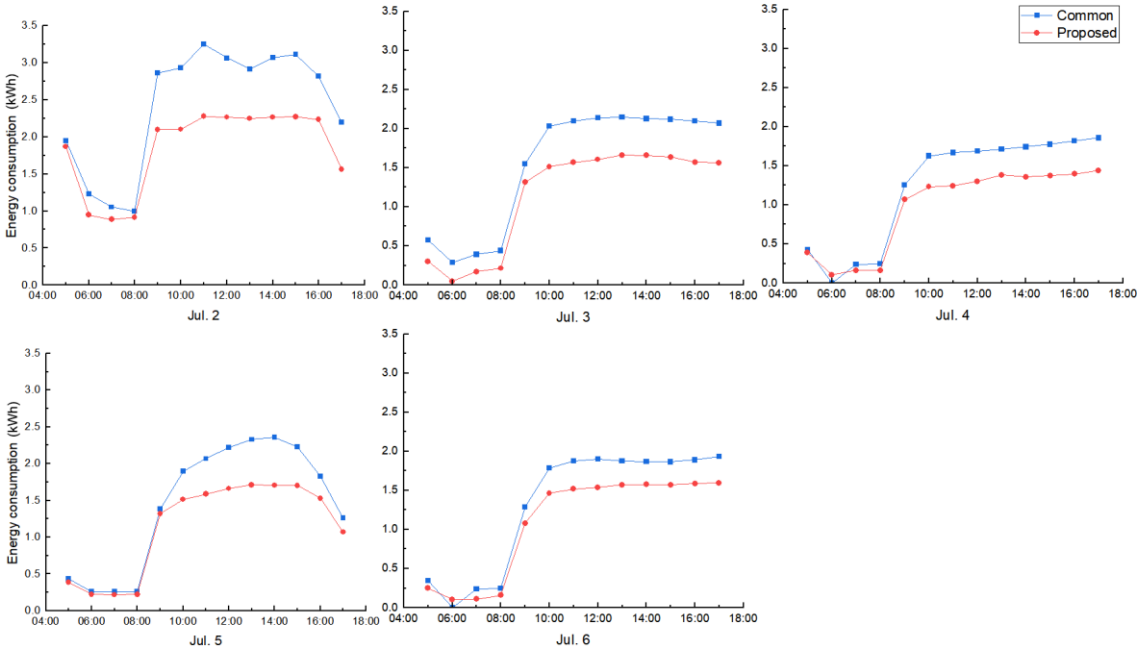

Fig. 22. Comparison of energy consumption using the common and proposed control strategies.

5. Discussion

In this paper, a TRNSYS building model and air conditioning system were established based on a previous experimental study conducted in an office building. The influence of the outdoor weather conditions on Q_{total} and the control measures to prevent condensation provide a reference, but the results cannot be generalized due to the specific thermophysical parameters of the experimental building. In subsequent studies, it is required to establish various building models with typical thermophysical parameters and compare the differences between different air conditioning systems for handling indoor heat and moisture loads.

Since this study focused on adjusting the operational parameters of the radiant floor and the ventilation system, the TRNSYS simulation platform used the multizone building module Type 56 to simplify the composite system model, and no other cooling plant was used. The energy consumption only considered the air-conditioning terminal, which was calculated using internal calculations of module Type 56. Although the simplified modeling method may cause deviations from the actual energy performance, the calculated energy consumption was highly similar to the measured data. Therefore, the accuracy of the simulation result can be ensured while reducing the computational complexity to improve the simulation efficiency. In subsequent research, we will include cooling equipment according to practical system configurations to establish a more accurate simulation model. The operational parameters of the equipment will be considered in the optimization process, and the energy performance will be investigated to provide a more applicable control method.

The study investigated the correlation between PMV, S_v/S_R, and energy consumption using simulations to develop a collaborative control strategy of the composite system. A data management tool was used to process the simulation data via filtering and integration to extract the characteristics of the data. It is necessary to explore the mathematical relationship between the data in more detail to obtain accurate and reliable processing results and improve the utilization value of the data. Moreover, jEPlus can be combined with an evolutionary algorithm that uses highly efficient and versatile multi-objective optimization algorithms (based on the popular NSGA-II) [54] for optimization problems in future studies.

Moreover, the PMV index has been challenged over time due to inaccurate prediction in laboratory experiment where air temperature, relative humidity and velocity are quite different from those in the real environment [55]. Many studies revealed the difference between PMV and Actual Mean Vote (AMV) in free-

running buildings [56,57]. Actually, the occupant adaptations were not considered in the PMV index, which overestimated the thermal sensation at high temperatures and underestimated the thermal sensation at low temperatures [58]. Therefore, PMV is not always the appropriate indicator due to its inaccuracy considering the impact of gender, age and other factors [59]. In the recent decades, the Adaptive Predicted Mean Vote (aPMV) model assumed that if a change occurs such as to produce discomfort, people react in ways which tend to restore their comfort has been gained significant attraction [60]. This model indicated that occupants were active participants to maintain thermal preferences instead of passive recipients of thermal environments [61]. Further study will take into account the aPMV index to objectively reflect the real response of occupants in order to achieve effective control of the indoor environment to avoid overcooling/overheating discomfort while reducing energy consumption in the combined RFC system and ventilation system.

The control strategies of the composite system used the RFC to remove the majority of the sensible heat load in the starting and operation stages. In contrast, the ventilation system control was used in response to changes in cooling energy demand, providing a better cooling performance than the RFC system due to the time delay of the RFC system. Therefore, novel automated intermittent control strategies will be added in a future study to take advantage of the dynamic thermal characteristics of the radiant structure. Moreover, critical adjustments should be made to the operational parameters, and the control time-step should be modified based on the system's operational performance and control performance to optimize the control process. Furthermore, it will be a challenge to apply the collaborative control strategy to a real-world scenario due to potential drawbacks in the control process and difficulties in fulfilling the requirements of various building types and climatic conditions. Real-time applications of complex optimization methods may result in longer computation times and worse control performance [62]. The sampling time should be determined through better estimate of the disturbance and overcoming the slow response of the radiant system, which further complicates the control problem. In a subsequent study, a controller design based on the collaborative control strategy applicable to real-world scenarios will be developed. It is crucial to assess the applicability of the optimization techniques and make necessary modifications in response to different environmental conditions and variable disturbances. Meanwhile, an analysis of the indoor thermal environment and an evaluation of indoor thermal comfort will be carried out to evaluate the practical application value and energy efficiency of the collaborative control strategy

6. Conclusions

jEPlus and TRNSYS were used to conduct simulations of the combined RFC and ventilation system in the starting and operation stages, and the simulation data were analyzed. Since the composite system had to cool the indoor environment, the cooling load sharing rate was the critical parameter impacting the integrated operational performance and indoor thermal comfort. The PMV was selected as the decision parameter due to its ability to reflect the control environment by considering the indoor air conditions and human behavior. An in-depth analysis of the correlation between S_v/S_R, PMV, and energy consumption indicated that the collaborative control strategy based on adjusting S_v/S_R according to the PMV value proved accurate.

In the starting stage, Q_{total} approximately doubled as the T_{ini} increased by 2 °C, exhibiting a significant increase. In addition, it was proved that the T_{ini} and φ_{ini} conditions had the largest impact on Q_{total} and were the dominant factors affecting the control of the composite system in the starting stage. Since the Q_{total} increased as the S_v/S_R decreased, an increase in Q_{total} primarily depended on enhancing the cooling capacity of the RFC system. The ventilation system should be started 1 hour earlier than the RFC system at the φ_{ini} of 85% to prevent condensation in the starting stage, whereas both systems should be started at the same time at the φ_{ini} of 75%.

In the operation stage, the maximum change in Q_{total} was about 0.2~0.5 kWh due to an increase in the internal heat gain. Thus, it was necessary to focus on the increased heat and moisture load caused by the higher internal heat gain. An increase in the S_v/S_R resulted in higher Q_{total}; thus, the cooling energy supply of the

composite system was improved by increasing the cooling capacity of the ventilation system.

The S_v/S_R increase and the PMV reduction resulted in higher energy consumption in the starting and operation stages, and a higher S_v/S_R level was required to improve indoor thermal comfort. Thus, it is required to minimize the S_v/S_R while ensuring acceptable indoor thermal comfort and reducing energy consumption. Moreover, it was found that V_{sa} and $t_{RFC\text{-}on}$ had a greater influence in the starting stage, whereas the effects of V_{sa} and T_{sa} were more significant in the operation stage. Based on the above evidence, a collaborative control strategy of the composite system was proposed. The strategy relied on the S_v/S_R adjustment based on the PMV-based prediction and achieved suitable changes in Q_{total}. Therefore, the composite system showed highly efficient cooling and energy conservation potential, with the highest energy saving of 26.2%.

Declaration of competing interest

The authors declare no potential conflicts of interest with respect to the research, authorship, and/or publication of this article.

CRediT author statement

Jing Ren: Software, Data curation, Writing - Original Draft, Formal analysis, Visualization. Jiying Liu: Conceptualization, Methodology, Supervision, Writing - Review & Editing, Project administration, Funding acquisition. Shiyu Zhou: Writing- Reviewing and Editing, Visualization. Moon Keun Kim: Writing- Reviewing and Editing. Jikui Miao: Writing- Reviewing and Editing, Project administration, Funding acquisition.

Acknowledgement

This work was funded by Natural Science Foundation of Shandong Province (ZR2021ME199) and Key Research and Development Project in Shandong Province (2018GSF121003). This work was also supported by the Plan of Introduction and Cultivation for Young Innovative Talents in Colleges and Universities of Shandong Province.

Nomenclature

E_{fan}	energy consumption of the fan (kWh)
E_{pump}	energy consumption of the water circulating pump (kWh)
g	acceleration of gravity (m/s^2)
H	water circulating pump head (m)
M_{sw}	supply water massive flow rate (kg/s)
P	supply air pressure (Pa)
$Q_{cl,dehum}$	the latent energy to dehumidify the air to set point humidity (kWh)
$Q_{cl,sens}$	the sensible energy to cool down the air to set point temperature (kWh)
$Q_{ht,reheat}$	sensible energy to reheat the air (kWh)
Q_{int}	internal heat gain (kW)
Q_{RFC}	the total cooling energy supplied by the RFC system (kWh)
Q_{total}	the total cooling energy supplied by the composite system (kWh)
Q_{vent}	the total cooling energy supplied by the ventilation system (kWh)
$t_{RFC\text{-}on}$	start time of RFC system
$t_{vent.\text{-}on}$	start time of second ventilation
T	temperature (°C)
T_{dp}	indoor air dew point temperature (°C)
T_f	floor surface temperature (°C)
T_{ini}	initial indoor air temperature (°C)
T_{mrt}	mean radiant temperature (°C)
T_{op}	operative temperature (°C)
$T_{our,dew}$	dewpoint temperature of outdoor air (°C)

$T_{out\text{-}max}$	maximum outdoor temperature (°C)
T_{set}	set point temperature (°C)
V_{sa}	supply air volume flow rate (m^3/s)
V_{sw}	supply water volume flow rate (m^3/s)
Δh_v	evaporation enthalpy (kJ/kg)

Subscripts

in	indoor air
out	outdoor air
sa	supply air
sw	supply water

Symbols

η_{fan}	fan efficiency
η_{pump}	water circulating pump efficiency
ρ_{sw}	density of supply water (kg/m^3)
φ	relative humidity (%)
φ_{ini}	initial indoor air relative humidity (%)
φ_{out}	outdoor air relative humidity (%)
$\varphi_{out\text{-}max}$	maximum outdoor air relative humidity (%)
ω	humidity ratio (g/kg)
ω_{max}	set point humidity ratio maximum (g/kg)

Reference

[1] Sui X, Zhang X, Effects of radiant terminal and air supply terminal devices on energy consumption of cooling load sharing rate in residential buildings, Energy Build. 49 (2012) 499-508.

[2] Liu J, Ren J, Zhang L, et al., Optimization of control strategies for the radiant floor cooling system combined with displacement ventilation: a case study of an office building in Jinan, China, Int. J. Archit. Eng. Techno. 6 (2019) 33-48.

[3] Saber E M, Tham K W, Leibundgut H, A review of high temperature cooling systems in tropical buildings, Build. Environ. 96 (2016) 237-249.

[4] Liu X, Zhang T, Tang H, et al., IEA EBC Annex 59: High temperature cooling and low temperature heating in buildings, Energy Build. 145 (2017) 267-275.

[5] Mohannad B, Method to integrate radiant cooling with hybrid ventilation to improve energy efficiency and avoid condensation in hot, humid environments, Build. 8 (2018) 69.

[6] Rhee K-N, Kim K W, A 50 year review of basic and applied research in radiant heating and cooling systems for the built environment, Build. Environ. 91 (2015) 166-190.

[7] Liu J, Kim M K, Srebric J, Numerical analysis of cooling potential and indoor thermal comfort with a novel hybrid radiant cooling system in hot and humid climates, Indoor Built Environ. 31 (2021) 929-943.

[8] Zhao K, Liu X, Ge J, Performance investigation of convective and radiant heat removal methods in large spaces, Energy Build. 208 (2020) 109650.

[9] Radwan A, Katsura T, Ding L, et al., Design and thermal analysis of a new multi-segmented mini channel based radiant ceiling cooling panel, J. Build. Eng. 40 (2021) 102330.

[10] KIM K W, Olesen B W, Radiant heating and cooling systems: part 1, ASHRAE J. 57 (2015) 28-37.

[11] Li Z, Zhang D, Chen X, et al., A comparative study on energy saving and economic efficiency of different cooling terminals based on exergy analysis, J. Build. Eng. 30 (2020) 101224.

[12] Jia H, Pang X, Haves P, Experimentally-determined characteristics of radiant systems for office buildings, Appl. Energy. 221 (2018) 41-54.

[13] Rhee K-N, Olesen B W, Kim K W, Ten questions about radiant heating and cooling systems, Build. Environ. 112 (2017) 367-381.

[14] de Wit A K, Wisse C J, Hydronic circuit topologies for thermally activated building systems – design questions and case study, Energy Build. 52 (2012) 56-67.
[15] Schmelas M, Feldmann T, Bollin E, Savings through the use of adaptive predictive control of thermo-active building systems (TABS): A case study, Appl. Energy. 199 (2017) 294-309.
[16] Ning B, Chen Y, Jia H, A response factor method to quantify the dynamic performance for pipe-embedded radiant systems, Energy Build. 250 (2021) 111311.
[17] Lim J-H, Song J-H, Song S-Y, Development of operational guidelines for thermally activated building system according to heating and cooling load characteristics, Appl. Energy. 126 (2014) 123-135.
[18] Liu J, Xie X, Qin F, et al., A case study of ground source direct cooling system integrated with water storage tank system, Build Simul. 9 (2016) 659-668.
[19] Bjarne W Olesen K S, Bjo rn Duchting, Control of slab heating and cooling systems studied by dynamic computer simulations, ASHRAE Transactions. 108 (2000) 698-707.
[20] Rhee K N, Yeo M S, Kim K W, Evaluation of the control performance of hydronic radiant heating systems based on the emulation using hardware-in-the-loop simulation, Build. Environ. 46 (2011) 2012-2022.
[21] Tang H, Raftery P, Liu X, et al., Performance analysis of pulsed flow control method for radiant slab system, Build. Environ. 127 (2018) 107-119.
[22] Ning B, Chen Y, Jia H, Cooling load dynamics and simplified calculation method for radiant ceiling panel and dedicated outdoor air system, Energy Build. 207 (2020) 109631.
[23] Liu J, Dalgo D A, Zhu S, et al., Performance analysis of a ductless personalized ventilation combined with radiant floor cooling system and displacement ventilation, Build Simul. 12 (2019) 905-919.
[24] Liu J, Li Z, Kim M K, et al., A comparison of the thermal comfort performances of a radiation floor cooling system when combined with a range of ventilation systems, Indoor Built Environ. 29 (2020) 527-542.
[25] Krusaa M R, Hviid C A, Combining suspended radiant ceiling with diffuse ventilation – Numerical performance analysis of low-energy office space in a temperate climate, J. Build. Eng. 38 (2021) 102161.
[26] Jin W, Jia L, Wang Q, et al., Study on Condensation Features of Radiant Cooling Ceiling, Procedia Eng. 121 (2015) 1682-1688.
[27] Zhang C, Pomianowski M, Heiselberg P K, et al., A review of integrated radiant heating/cooling with ventilation systems- Thermal comfort and indoor air quality, Energy Build. 223 (2020) 110094.
[28] Hao X, Zhang G, Chen Y, et al., A combined system of chilled ceiling, displacement ventilation and desiccant dehumidification, Build. Environ. 42 (2007) 3298-3308.
[29] Zhang T, Liu X, Jiang Y, Development of temperature and humidity independent control (THIC) air-conditioning systems in China—A review, Renew. Sustain. Energy Rev. 29 (2014) 793-803.
[30] Romaní J, de Gracia A, Cabeza L F, Simulation and control of thermally activated building systems (TABS), Energy Build. 127 (2016) 22-42.
[31] Wu J, Li X, Lin Y, et al., A PMV-based HVAC control strategy for office rooms subjected to solar radiation, Build. Environ. 177 (2020) 106863.
[32] Li B, Du C, Tan M, et al., A modified method of evaluating the impact of air humidity on human acceptable air temperatures in hot-humid environments, Energy Build. 158 (2018) 393-405.
[33] Xu Z, Hu G, Spanos C J, et al., PMV-based event-triggered mechanism for building energy management under uncertainties, Energy Build. 152 (2017) 73-85.
[34] Saber E M, Iyengar R, Mast M, et al., Thermal comfort and IAQ analysis of a decentralized DOAS system coupled with radiant cooling for the tropics, Build. Environ. 82 (2014) 361-370.
[35] Zarrella A, De Carli M, Peretti C, Radiant floor cooling coupled with dehumidification systems in residential buildings: A simulation-based analysis, Energy Convers. Manage. 85 (2014) 254-263.

[36] Qin S Y, Cui X, Yang C, et al., Thermal comfort analysis of radiant cooling panels with dedicated fresh-air system, Indoor Built Environ. 30 (2020) 1596-1608.
[37] Gu X, Cheng M, Zhang X, et al., Performance analysis of a hybrid non-centralized radiant floor cooling system in hot and humid regions, Case Stud. Therm. Eng. 28 (2021) 101645.
[38] Hu Y, Xia X, Wang J, Research on operation strategy of radiant cooling system based on intermittent operation characteristics, J. Build. Eng. 45 (2022) 103483.
[39] Crawley D B, Hand J W, Kummert M, et al., Contrasting the capabilities of building energy performance simulation programs, Build. Environ. 43 (2008) 661-673.
[40] Trnsys. Transient system simulation tool, Solar Energy Lab. Available online: http://www.trnsys.com/.
[41] jEPlus. Parametric analysis tool. Available online: http://www.jeplus.org/wiki/doku.php.
[42] Liu J, Zhu X, Kim M K, et al., A transient two-dimensional CFD evaluation of indoor thermal comfort with an intermittently-operated radiant floor heating system in an office building, Int. J. Archit. Eng. Techno. 7 (2020) 62-87.
[43] Ren J, Liu J, Zhou S, et al., Experimental study on control strategies of radiant floor cooling system with direct-ground cooling source and displacement ventilation system: A case study in an office building, Energy. 239 (2022) 122410.
[44] Fanger P O. Thermal comfort. Copenhagen: Danish Technical Press, 1970.
[45] Liu X, Zhang T, Zhou X, et al. Radiant Cooling. China Architecture & Building Press, 2019.
[46] ASHRAE. ASHRAE 55-2013: thermal environmental conditions for human occupancy. Atlanta: ASHRAE, 2013.
[47] Feng J, Schiavon S, Bauman F, New method for the design of radiant floor cooling systems with solar radiation, Energy Build. 125 (2016) 9-18.
[48] Lu Y. Practical heating and air conditioning design manual. China Architecture & Building Press, 2008.
[49] Annual report on China building energy efficiency. China Architecture & Building Press, 2014.
[50] Ren J, Su M, Zhao X, et al., Experimental study on the dynamic thermal response of a radiant floor system in an office building, E3S Web Conf. 246 (2021) 10003.
[51] Royapoor M, Roskilly T, Building model calibration using energy and environmental data, Energy Build. 94 (2015) 109-120.
[52] ASHRAE. ASHRAE Guideline 14-2002: Measurement of Energy and Demand Savings. Atlanta: ASHRAE, 2002.
[53] Feng J, Schiavon S, Bauman F, Cooling load differences between radiant and air systems, Energy Build. 65 (2013) 310-321.
[54] Aghamolaei R, Ghaani M R, Balancing the impacts of energy efficiency strategies on comfort quality of interior places: Application of optimization algorithms in domestic housing, J. Build. Eng. 29 (2020) 101174.
[55] Bouden C, Ghrab N, An adaptive thermal comfort model for the Tunisian context: a field study results, Energy Build. 37 (2005) 952-963.
[56] Yao R, Li B, Liu J, A theoretical adaptive model of thermal comfort – Adaptive Predicted Mean Vote (aPMV), Build. Environ. 44 (2009) 2089-2096.
[57] Yang Y, Li B, Liu H, et al., A study of adaptive thermal comfort in a well-controlled climate chamber, Appl. Therm. Eng. 76 (2015) 283-291.
[58] Yao R, Zhang S, Du C, et al., Evolution and performance analysis of adaptive thermal comfort models – A comprehensive literature review, Build. Environ. 217 (2022) 109020.
[59] Yuan F, Yao R, Sadrizadeh S, et al., Thermal comfort in hospital buildings – A literature review, J. Build. Eng. 45 (2022) 103463.
[60] Nicol J F, Humphreys M A, Adaptive thermal comfort and sustainable thermal standards for buildings, Energy Build. 34 (2002) 563-572.
[61] Dear R D, Brager G, Developing an adaptive model of thermal comfort and preference, ASHRAE Trans. 104

(1998) 73-81(9).
[62] Yao Y, Shekhar D K, State of the art review on model predictive control (MPC) in Heating Ventilation and Air-conditioning (HVAC) field, Build. Environ. 200 (2021) 107952.